$5f^N-5f^{N-1}6d^1$ Transitions of U^{3+} and U^{4+} Ions in High-symmetry Sites

Mirosław Karbowiak* and Janusz Drożdżyński

Faculty of Chemistry, University of Wrocław, ul. F. Joliot-Curie 14, 50-383 Wrocław, Poland

Received: December 27, 2003; In Final Form: April 26, 2004

$5f^N \rightarrow 5f^{N-1}6d^1$ absorption spectra of U^{4+}- and U^{3+}-doped Cs_2NaYCl_6, Cs_2LiYCl_6, Cs_2NaYBr_6, $CsCdBr_3$, and $Cs_3Lu_2Cl_9$ single crystals were recorded at 4.2 K in the 14 000−50 000 cm^{-1} spectral range. The $5f^2 \rightarrow 5f^16d^1$ absorption bands of U^{4+} ions were observed in the 30 000−37 000 cm^{-1} energy range, and have been assigned as transitions from the $^3H_4$ ground multiplet of the $5f^2$ configuration to crystal-field levels of the $5f^16d(t_{2g})^1$ manifold. The energies of the lowest levels of the $5f^16d(t_{2g})^1$ configuration have been for the first time determined for U^{4+} ions doped in a chloride or bromide host crystal. They are equal to 26 360 and 28 590 cm^{-1} for U^{4+}:$CsCdBr_3$ and U^{4+}:Cs_2NaYBr_6 respectively and range from 30 360 to 31 010 cm^{-1} for U^{4+} doped in the chloride hosts. Highly structured vibronic bands of $5f^3 \rightarrow 5f^26d(t_{2g})^1$ absorption transitions of the U^{3+} ions appeared at an energy as low as 14 158 cm^{-1}, and have been assigned to transitions from the $^4I_{9/2}$ ground multiplet of the $5f^3$ configuration to crystal-field levels arising from the configurations $5f^2(^3H_4)6d(t_{2g})^1(\Gamma_{8g})$ (barycenter at ∼16 000 cm^{-1}) and $5f^2(^3H_4)6d(t_{2g})^1(\Gamma_{7g})$ (barycenter at ∼19 000 cm^{-1}). Besides, some low intensity bands observed at ∼18 600 and above 21 000 cm^{-1} have been assigned as transitions to the $5f^2(^3F_2)6d(t_{2g})^1(\Gamma_{8g})$ and $5f^2(^3F_2)6d(t_{2g})^1(\Gamma_{7g})$ levels, respectively. Transitions to the $5f^26d(e_g)^1$ levels of U^{3+} ions have been observed as broad and unstructured bands at wavenumbers higher than 38 000 cm^{-1}. The crystal field splitting ($10Dq$) of the $5f^26d^1$ configuration for U^{3+} doped in Cs_2NaYCl_6 single crystals amounts to ∼23 000 cm^{-1}, and the separation between Γ_{8g} and Γ_{7g} components of the t_{2g} state, resulting from spin−orbit interaction for the 6d electron, can be evaluated as 3350 cm^{-1}. The splitting of the $5f^2(^{2S+1}L_J)6d(\gamma)^1(\Gamma_{ig})$ ($\gamma = t_{2g}$ or e_g; $i = 7$ or 8) configurations, resulting from the coupling of the $5f^2$ core electrons with the 6d electron is somewhat smaller and amounts to ∼3000 cm^{-1}. The main feature of the crystal level structure observed in the $5f^3-5f^26d^1$ absorption spectra of U^{3+} ions reflects the dominating influence of the crystal field splitting and spin−orbit coupling of the 6d electron.

1. Introduction

The energy levels of the $5f^3$ configuration for U^{3+} ions doped in a number of single crystals[1−5] and polycrystalline samples[6−8] have been relatively well characterized and understood in terms of theoretical models.[9−11] The $5f^3$ configuration extends up to about 45 000 cm^{-1}, but the sharp lines of intraconfigurational $5f^3 \rightarrow 5f^3$ transitions could be merely assigned in 4000−20 000 cm^{-1} energy range, as at higher energies they are obscured by strong and broad absorption bands due to parity-allowed $5f^3 \rightarrow 5f^26d^1$ transitions.

In the absorption spectra of UX_3 halides (X = F, Cl or Br)[12] as well as LaX'_3:U^{3+} (X′ = Cl or Br)[4] and $LiYF_4$:U^{3+} single crystals[13] the $5f^3 \rightarrow 5f^26d^1$ transitions appear at relatively high energies of about 20 000 cm^{-1}. Uranium(3+) chloro- or bromo-complexes with a somewhat more covalent uranium-ligand bonds exhibit the $5f^3 \rightarrow 5f^26d^1$ transitions at energies as low as ∼14 200 cm^{-1}, which considerably limits the spectral region suitable for an analysis of $5f^3 \rightarrow 5f^3$ transition. On the other hand it makes the $5f^3 \rightarrow 5f^26d^1$ transitions more accessible experimentally as compared e.g. with Ln^{3+} ions, for which the $4f^N \rightarrow 4f^{N-1}5d$ absorption bands are observed in the UV and VUV regions, at much higher energies.

So far, analyses of f−d transitions have been mainly reported for lanthanide ions. In most cases the structure of the observed $4f^N \rightarrow 4f^{N-1}5d^1$ transitions have been rationalized in the simple one-electron model[14,15] or with the assumption, that the excited configurations were formed by a coupling of the split by the crystal-field 5d orbitals with the $4f^{N-1}$ core electrons and lattice vibrations.[16,17,18,19] Recently, $4f^N \rightarrow 4f^{N-1}5d^1$ transitions of Ln^{3+} ions incorporated in $LiYF_4$, CaF_2, and YPO_4 host lattices have been recorded in the UV and VUV spectral region (100−250 nm) and were analyzed. For the calculation of the $4f^{N-1}5d^1$ energy levels has been applied a theoretical model, which extends the established one for the $4f^N$ configuration by including crystal-field and spin−orbit interactions for the 5d electron as well as the Coulomb interaction between the 4f and 5d electrons.[20,21,22]

For actinide ions reported analyses of f−d transitions are scarce. Hitherto, Pa^{4+}:Cs_2ZrCl_6 may be regarded as the only one well-characterized system for which low-temperature $5f^1 \rightarrow 6d^1$ absorption and $6d^1 \rightarrow 5f^1$ emission spectra were measured and analyzed.[23,24] On the basis of ab initio calculations, an excellent overall agreement between the theoretical and experimental 5f and 6d energy levels has been obtained.[25] Besides, $6d^1 \rightarrow 5f^1$ luminescence of Pa^{4+} ions in $ThBr_4$ and $ThCl_4$ single crystals[26] and UV luminescence due to $5f^16d^1 \rightarrow 5f^2$ transitions in U^{4+}-doped $LiYF_4$ crystals have been reported.[27,28]

Since the 6d orbitals have a larger spatial extend than those of 5f, most of the f−d transition intensities are incorporated in broad vibronic bands. In the case of the U^{3+} ion an additional complication results from the large number of $5f^3$ levels observed in the region of f−d transitions. The overlapping of $5f^3$ L′S′J′ multiplets gave rise to relatively broad and strong

* Corresponding author. E-mail: karb@wchuwr.chem.uni.wroc.pl. Telephone: +48 71 3757304. Fax: +48 3282348.

10.1021/jp038024q CCC: $27.50
Published on Web 07/02/2004

f−f bands, superimposed on the envelope of f−d bands, which makes the analysis of f−d spectra difficult, especially for hosts with a low site symmetry, where the f−f and f−d transition intensities are comparable.

The first attempts of an analysis of uranium(3+) $5f^3 \rightarrow 5f^26d^1$ transitions have been reported for solution spectra by Kaminskaya et al.[29,30] and for solid state by Mazurak et al.[31] An interpretation of the $5f^3 \rightarrow 5f^26d^1$ bands observed in room-temperature absorption spectrum of U^{3+}-doped Cs_2NaYCl_6 single crystals have been presented in ref 32. The interpretation is based on the assumption that the $5f^26d^1$ configuration behaves according to the $J_1\gamma_n$ coupling scheme, where J_1 is the total angular momentum of a Russell−Saunders term derived for the $5f^2$ core and $J_1\gamma_n$ is a state of the 6d electron in the crystal-field. However, as we shall show in this paper the bands observed in 30 000−37 000 cm^{-1} energy range, assigned in ref 32 to the U^{3+} ion, are in fact f−d transitions of U^{4+} impurities. The 5 K absorption spectrum showing the $5f^3 \rightarrow 5f^26d^1$ transitions of U^{3+}:Cs_2NaYCl_6 in the 14 000−17 500 cm^{-1} spectral range was reported in ref 33. The authors stated that the spectrum in this region is dominated by electric dipole vibronic satellites built on the envelope of a vibrational progression combined with the a_{1g} mode. It has been assumed that this vibronic sequence is observed up to the 10th a_{1g} progression. The performed assignment was next corrected in ref 3 and three zero-phonon lines were derived in 14 000−17 500 cm^{-1} energy range. Low-temperature absorption spectra showing f−d transitions of U^{3+} ions in Cs_2LiYCl_6 (ref 3) and Cs_2NaYBr_6 (ref 34) single crystals have been also presented. Energies of a number of zero-phonon lines have been determined but no farther analysis have been attempted.

In this paper an analysis of low-temperature absorption spectra recorded in 14 000−50 000 cm^{-1} energy range for U^{3+} and U^{4+} ions doped in Cs_2NaYCl_6, Cs_2LiYCl_6, Cs_2NaYBr_6, $CsCdBr_3$, and $Cs_3Lu_2Cl_9$ single crystals is presented. The Cs_2NaYCl_6, Cs_2LiYCl_6, and Cs_2NaYBr_6 elpasolites are isostructural and possess the cubic $Fm3m$ type of symmetry. In these crystals the Y^{3+} ions are surrounded by an octahedral array of six chloride ions. The $CsCdBr_3$ crystals have the hexagonal structure of $CsNiCl_3$, with the space group $P63/mmc$(D^4_{6h}) and two formula units per unit cell.[35] The crystal structure can be described as infinite linear chains of face sharing $(CdBr_6)^{4-}$ octahedra along the crystallographic c axis, with charge compensating Cs^+ ions located between the chains. Trivalent lanthanide ions are incorporated into this host predominantly as pairs replacing three adjacent Cd^{2+} ions to form dimer centers of the type $-Cd^{2+}-Ln^{3+}-$vacancy$-Ln^{3+}-Cd^{2+}-$ (refs 36 and 37). Both of the Ln^{3+} ions in these symmetric pairs possess the C_{3v} site symmetry. $Cs_3Lu_2Cl_9$ crystallize in the trigonal space group $R3c$ (ref 38). The structure is built up of $[Lu_2Cl_9]^{3-}$ dimers, which contain two face-sharing $LuCl_6^{3-}$ octahedra. The Lu^{3+} ions occupy sites of C_{3v} symmetry.

Thus, the common feature of all investigated host lattices are MX_6^{3-} octahedra. In the elpasolites the U^{3+} ions substitute for Y^{3+} in a site of pure O_h site symmetry. In the two other host lattices the U^{3+} ions possess the C_{3v} site symmetry, but the C_{3v} crystal field can be described as a superposition of a dominant octahedral part and a weaker trigonal one.[39] The trigonal distortion is larger for $Cs_3Lu_2Cl_9$ host crystals as compared with those of $CsCdBr_3$.

In the elpasolites, due to the presence of a center of inversion the $5f^3 \rightarrow 5f^3$ transitions are forbidden and do not interfere with $5f^3 \rightarrow 5f^26d^1$ transitions. Since in the $CsCdBr_3$ and $Cs_3Lu_2Cl_9$ crystals the trigonal distortion is small, the splitting of the 6d orbital due to the lowering of the site symmetry from O_h to C_{3v} should be also relatively small and one may expect some common features in the $5f^3 \rightarrow 5f^26d^1$ absorption spectra of all investigated compounds. In view of the limited number of available experimental energy levels as compared with that of adjustable parameters we have not attempted to reproduce the observed $5f^26d^1$ energy levels structure in terms of the extended parametric Hamiltonian, recently applied for lanthanide ions.[21,22] Instead of that we prefer to present an empirical interpretation in terms of a simple model assuming the coupling of crystal-field levels of the $6d^1$ electron with the lattice and the multiplet structure of the $5f^{N-1}$ configuration. Since in this simple model the combined effects of the Coulomb coupling of $6d^1$ electron with the $5f^{N-1}$ core electrons are neglected, it may obviously not be possible to explain all details of the fine features observed in the spectra. Nevertheless, the general structure of the spectra may be accounted for, and the main characters of the excited states of the $5f^{N-1}6d^1$ manifold, which are giving rise to a particular group of energy levels, could be assigned. Just recently, a paper reporting ab initio theoretical studies on the structure and spectroscopy of U^{3+} in Cs_2NaYCl_6 single crystals has appeared,[40] which enabled us to show relations between some of our experimental findings and the results of theoretical calculations.

2. Experimental Section

Uranium(3+)-doped single crystals were grown by the Bridgman-Stockbarger method. The starting materials for synthesis of the investigated crystals were the appropriate binary halides. YCl_3, YBr_3, and $LuCl_3$ were prepared by the ammonium chloride route[41] using the corresponding rare earth oxides M_2O_3, NH_4Cl or NH_4Br and concentrated hydrochloric or hydrobromic acid. The Cs_2NaYCl_6, Cs_2LiYCl_6, and Cs_2NaYBr_6 crystals with a nominal 0.05 mol % uranium concentration were obtained using Cs_2NaUCl_6, Cs_2LiUCl_6, and Cs_2NaUBr_6 as the doping substances, respectively. For the preparation of these complex compounds a well ground stoichiometric mixture of CsCl or CsBr and UCl_3 or UBr_3 was in a quartz tube sealed under vacuum. UCl_3 and UBr_3 have been obtained by thermal decomposition of $NH_4UCl_4 \cdot 4H_2O$ and $(NH_4)_2UBr_5 \cdot 2CH_3CN \cdot 5H_2O$ according to procedures reported in refs 42 and 43, respectively. The mixture was next heated at 400 °C for 3 days. Ink-blue fine crystalline powders were obtained. The doped single crystals were cut and polished under dry paraffin oil. For the absorption spectra measurements, 1 mm thick plates (∼6 mm in diameter) were used.

U^{3+}-doped $CsCdBr_3$ single crystals of a nominal 0.2 mol % uranium concentration were grown using UBr_3 as the doping substance. However, some segregation of the doped substance observed during the crystal growth may somewhat lower this concentration. Samples of approximately 1 mm thick were cleaved from the bulk crystal. UCl_3 was used as the uranium(3+) source during growth of (0.25 mol %) U^{3+}:$Cs_3Lu_2Cl_9$ crystals. Plates of about 5 mm in diameter and 1 mm thick were cut from the bulk crystal and polished under a dry paraffin oil. The absorption spectra were recorded on a Cary-50 UV−vis−NIR spectrophotometer in the 14 000−50 000 cm^{-1} range. An Oxford Instrument model CF1204 cryostat was used for low-temperature measurements.

3. Results

Figure 1a presents the room-temperature absorption spectrum of U^{3+}:Cs_2NaYCl_6 single crystal in the f−d spectral range. Three groups of bands, labeled in Figure 1 as I, II, and III could be

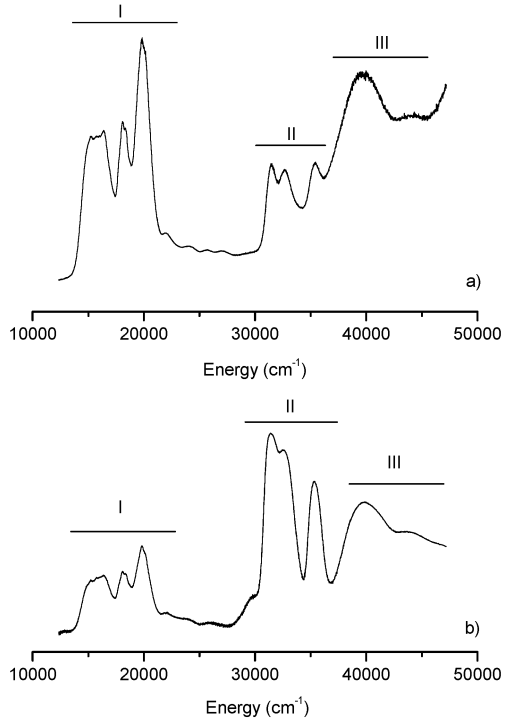

Figure 1. Room-temperature absorption spectra of Cs_2NaYCl_6 single crystals doped with Cs_2NaUCl_6 (a) and UCl_4 (b) measured in the $5f^N \rightarrow 5f^{N-1}6d^1$ transition range. The group of bands marked as I and III are due to $5f^3 \rightarrow 5f^26d^1$ transitions of U^{3+} ions, while the group II should be assigned to $5f^2 \rightarrow 5f^16d^1$ transitions of U^{4+} ion.

distinguished. In a previous semiempirical analysis,[32] the bands of group II have been erroneously attributed to f−d transitions of the U^{3+} ion. Figure 1b presents the same spectrum as in Figure 1a, but measured for a UCl_4-doped Cs_2NaYCl_6 single crystal. During the crystal growth usually a partial reduction of U^{4+} to U^{3+} occurs, resulting in the presence of both valence states. However, in the spectrum presented in Figure 1b, the relative intensities of the bands labeled as II are higher than those of I and III, which indicates that the first ones are due to U^{4+} ions. Hence, only the bands labeled as I and III may be recognized as characteristic for U^{3+} ions. In a number of measurements performed for Cs_2NaYCl_6 crystals doped with Cs_2NaUCl_6 we have noticed also a direct relationship between the concentration of the U^{3+} ions and the band intensities of group I and III while those of II in relation to I and III were different, which proves our conclusion.

A survey of the investigated absorption spectra in the 14 000−50 000 cm^{-1} spectral range at 4.2 K is presented in Figure 2. Similar to the observation in the room-temperature absorption spectrum of U^{3+}:Cs_2NaYCl_6, one may distinguish in this region three groups of absorption bands. Groups I and II consist of strong bands with a fine structure. Those forming group III are also relatively intense but do not possess a fine structure. In the 21 000−27 000 cm^{-1} energy range one may observe a number of bands (group IV) with a fine structure, but with an intensity about 1 order of magnitude lower as compared with those of group I or III. Linking the low-temperature spectra with those recorded in room temperature (Figure 1), one may attribute the bands forming group II to f−d transitions of U^{4+} ions, while those of groups I, III, and IV may be attributed to the U^{3+} ion.

3.1. Transitions of U^{4+} Ions. The absorption bands labeled as group II in Figure 2 are due to U^{4+} transitions from the lowest crystal field component of the $^3H_4$ ground multiplet of the $5f^2$ configuration to energy levels of the $5f^16d(t_{2g})^1$ manifold. In somewhat more detail they are presented in Figure 3. In all

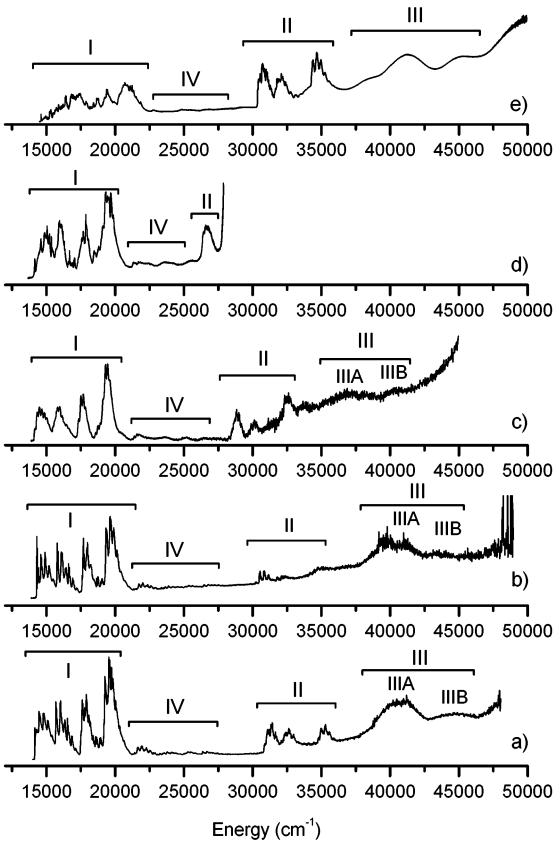

Figure 2. Survey absorption spectra at 4.2 K of Cs_2NaYCl_6 (a), Cs_2LiYCl_6 (b), Cs_2NaYBr_6 (c), $CsCdBr_3$ (d), and $Cs_3Lu_2Cl_9$ (e) single crystals doped with U^{3+} ions.

chloride host crystals the first $5f^2 \rightarrow 5f^16d(t_{2g})^1$ transitions appear at a similar energy equal to 31 010, 30 500, and 30 360 cm^{-1} for Cs_2NaYCl_6, Cs_2LiYCl_6, and $Cs_3Lu_2Cl_9$, respectively. The differences results from a somewhat different covalency (nepheloauxetic effect) of the host crystals and the strength of the crystal field which splits the $5f^16d^1$ configuration into t_{2g} and e_g components. For the more covalent bromide hosts, the shift of the $5f^2 \rightarrow 5f^16d(t_{2g})^1$ bands toward the infrared region is more pronounced and first transitions are observed at 28 590 cm^1 for Cs_2NaYBr_6 and as low as 26 360 cm^{-1} for the most covalent among the $CsCdBr_3$ crystals.

The spectra of all investigated crystals are similar, composed of three broad bands with a fine structure superimposed on them. Transitions to the lowest energy levels of U^{4+} in $CsCdBr_3$ could be observed only, owing to the appearance at ∼28 000 cm^{-1} of a strong bands of the host lattice absorption edge. The fine structure has been most distinctly exhibited in the spectrum of U^{4+}:$Cs_3Lu_2Cl_9$. Figure 4 presents in detail the lowest-energy absorption band of U^{4+}:$Cs_3Lu_2Cl_9$ due to $5f^2 \rightarrow 5f^16d(t_{2g})^1$ transitions in the 30 300−31 600 cm^{-1} energy range. The zero-phonon (ZP) line is placed at 30 362 cm^{-1}. The most prominent feature of the absorption band is the vibronic progression based on the $\nu_1(a_{1g})$ even mode of 308 cm^{-1} energy. The zero-phonon line is accompanied by electric-dipole vibronic satellites shifted from it by 48, 86, 134, 188, and 247 cm^{-1} (average values). For the bands with barycenters at ∼32 000 and 34 600 cm^{-1} (Figure 3) the vibronic satellites are observed at the same frequencies as listed above. One may note, however, a lower resolution of the last band. The positions of the zero-phonon lines have been determined at 31 780 and 34 290 cm^{-1}.

For the U^{4+}:Cs_2NaYCl_6 crystals (Figure 3a) three structured bands could be easily distinguished with zero-phonon lines at

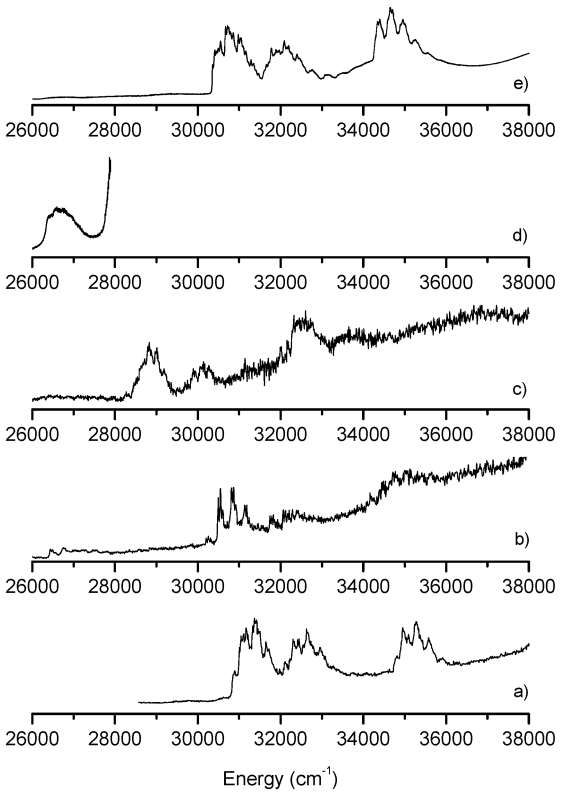

Figure 3. 4.2 K absorption spectra of Cs_2NaYCl_6 (a), Cs_2LiYCl_6 (b), Cs_2NaYBr_6 (c), $CsCdBr_3$ (d), and $Cs_3Lu_2Cl_9$ (e) single crystals doped with U^{3+} ions. The figure shows the spectral region of $5f^2 \rightarrow 5f^16d(t_{2g})^1$ transitions of U^{4+} ions, which are present in these crystals as impurities.

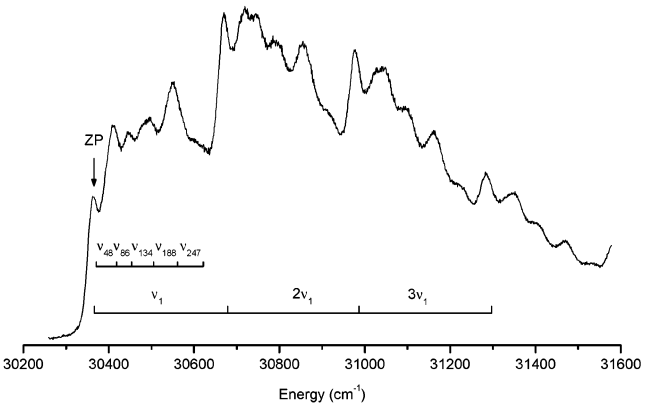

Figure 4. Lowest-energy $5f^2 \rightarrow 5f^16d^1$ absorption band of U^{4+} in the $Cs_3Lu_2Cl_9$ single crystal measured at 4.2 K. The arrow indicates the lowest energy zero-phonon (ZP) line. The vibronic sidebands are shifted by $\nu_i = 48$, 86, 134, 188, and 247 cm^{-1} from the zero-phonon line. Vibronic progression is seen, which arises from the 308 cm^{-1} totally symmetric $\nu_1(a_{1g})$ stretch of the UCl_6^{3-} moiety.

31 010, 32 295, and 34 960 cm^{-1}. Vibronic satellites have been observed at 40, 65, 88, 121, 161, 224, and 262 cm^{-1}. The vibronic progression is based on the a_{1g} mode of the 320 cm^{-1} energy.

In the case of U^{4+}:Cs_2LiYCl_6 crystals (Figure 3b) the $5f^2 \rightarrow 5d^16d(t_{2g})^1$ absorption bands are weak and only the position of the first zero-phonon line at 30 500 cm^{-1} could be determined. The frequencies of vibronic satellites coupled to this line are equal to 53, 108, 161, and 214 cm^{-1}. The vibronic progression is based on the mode of 315 cm^{-1} energy.

The zero-phonon lines for the U^{4+}:Cs_2NaYBr_6 single crystals (Figure 3c) were determined at 28 590, 29 840, and 32 300 cm^{-1}. The vibronic satellites are shifted by 42, 65, 95, and 140 cm^{-1} from the ZP line, and vibronic progression is based on the 180 cm^{-1} a_{1g} mode.

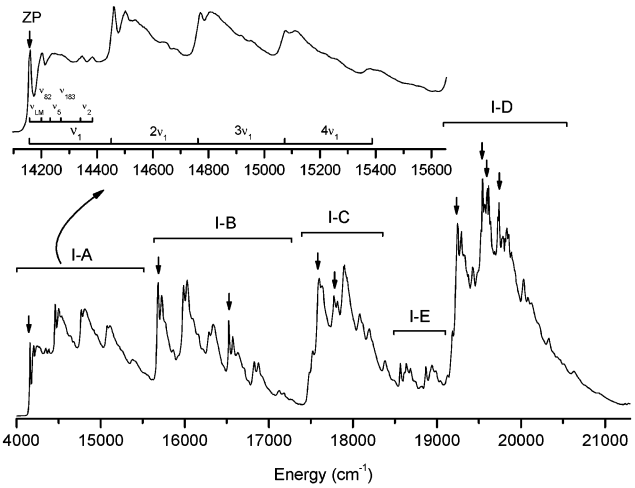

Figure 5. Absorption spectrum recorded at 4.2 K for the U^{3+}:Cs_2NaYCl_6 single crystal in the $^4I_{9/2} \rightarrow 5f^26d(t_{2g})^1$ transition range. The zero-phonon lines are indicated by arrows. In the inset the lowest energy absorption band is presented in extended *x*-axis scale. The vibronic sidebands are shifted by $\nu_{LM} = 45$, $\nu_{82} = 82$, $\nu_5 = 120$, $\nu_{183} = 183$, and $\nu_2 = 230$ cm^{-1} from the zero-phonon lines. Vibronic progression is seen, which arises from the 304 cm^{-1} totally symmetric $\nu_1(a_{1g})$ stretch of the UCl_6^{3-} moiety.

TABLE 1: Energies of Zero-Phonon Lines Observed for the $^3H_4 \rightarrow 5f^16d(t_{2g})^1$ Transitions of U^{4+}

host lattice	energies of zero-phonon lines (cm^{-1})		
Cs_2LiYCl_6	30 500		
Cs_2NaYCl_6	31 010	32 295	34 960
$Cs_3Lu_2Cl_9$	30 360	31 780	34 290
Cs_2NaYBr_6	28 590	29 840	32 300
$CsCdBr_3$	26 360		

For the U:$^4CsCdBr_3$ crystal (Figure 3d) transitions to $5f^56d(t_{2g})^1$ levels of the lowest energy could be observed only. The vibronic satellites which are forming the band with the barycenter at ~26 600 cm^{-1} are not well separated, and a vibronic progression based on the 160 cm^{-1} a_{1g} mode could be only distinguished. The energy of zero-phonon line has been determined at 26 360 cm^{-1}. At an energy of ~280 000 cm^{-1} very intense transition due to the cutoff of the host crystal appear.

The determined positions of $5f^2 \rightarrow 5f^56d(t_{2g})^1$ zero-phonon lines for U^{4+} in all investigated crystals are summarized in Table 1.

3.2. Transitions of U^{3+} Ions. The lines observed in the 14 000−21 000 cm^{-1} range (Figure 2, group I) are assigned as transitions from the $^4I_{9/2}$ ground multiplet to $5f^26d(t_{2g})^1$ crystal field levels of U^{3+} ions. The most prominent vibronic feature is the a_{1g} progression built on each of the zero-phonon lines. Besides, an additional fine structure has been observed due to electric-dipole vibronic transitions. The broad bands without a fine structure, observed in the 37 000−47000 cm^{-1} range (Figure 2, group III) have been assigned as transitions to the $5f^26d(e_g)^1$ crystal field levels of U^{3+}.

3.2.1. U^{3+}:Cs_2NaYCl_6. Figure 5 shows in detail the absorption spectrum of U^{3+}:Cs_2NaYCl_6 in the $^4I_{9/2} \rightarrow 5f^26d(t_{2g})^1$ transition range. The spectrum consists of four main bands, labeled as I-A, I-B, I-C, and I-D with barycenters at ~15 000, 16 200, 18 000, and 19 800 cm^{-1}, respectively. The major feature of the spectrum is the 304 cm^{-1} vibronic progression which arises from the totally symmetric $\nu_1(a_{1g})$ stretch of the UCl_6^{3-} moiety. For the band I-A the first zero-phonon line is

distinctly observable at 14 158 cm^{-1}. For this line the $\nu_1(a_{1g})$ progression extends at least through four quanta. On this progression are superimposed also other vibronic electric dipole transitions displaced from the zero-phonon line by 45, 82, 120, 183, and 230 cm^{-1} (average values). The ground state for the $5f^5$ configuration of U^{3+} ions is $1\Gamma_{8u}$ ($^4I_{9/2}$). The $5f^26d^1$ configuration splits into Γ_{6g}, Γ_{7g}, and Γ_{8g} crystal field levels. One may expect therefore that most of the vibronic sidebands intensity will arise from even parity vibrations. From an analysis of Raman and IR spectra three even modes of the $Y(U)Cl_6^{3-}$ complex anion have been assigned as $\nu_1(a_{1g}) \approx 287$ cm^{-1}, $\nu_2(e_g) \approx 227$ cm^{-1}, and $\nu_5(t_{2g}) \approx 127$ cm^{-1} (ref 33). Besides, one may expect the appearance of lower energy lattice modes. Hence, the lines observed in the investigated spectrum at 230 and 120 cm^{-1} ought to be assigned as $\nu_2(e_g)$ and $\nu_5(t_{2g})$, respectively. The line at 45 cm^{-1} may be assigned as a lattice mode (ν_{LM}). The two lines at $\nu_{82} = 82$ and $\nu_{183} = 183$ cm^{-1} are most probably combination bands and could be assigned as $2\nu_{LM}$ and $4\nu_{LM}$, respectively. The zero-phonon line together with the vibronic sidebands form a characteristic vibronic pattern which is helpful for identification of other zero-phonon lines.

In band I-B, two zero-phonon lines could be readily localized at 15 684 and 16 524 cm^{-1}. Progressions up to the second one, based on the a_{1g} mode, are easily perceptible for both lines. For the band I-C observed at ∼18 000 cm^{-1} the positions of two zero-phonon lines can be deduced at 17 597 and 17 774 cm^{-1}. In the I-D band with the barycenter at ∼19 900 cm^{-1}, the vibronic pattern is not so clearly resolved as it was for lower energy bands. Nevertheless, the positions of four zero-phonon lines were determined at 19 250, 19 544, 19 568, and 19 740 cm^{-1}. However, some lines observed in this band could not be assigned which may suggest that in this spectral region other, nonidentified zero-phonon transitions may be present.

Besides, a group of low intensity bands, but with a well resolved fine structure, has been observed in the 18 500−19 100 cm^{-1} energy region (group I-E). The first band of this group is composed of vibronic electric dipole transitions coupled to the zero-phonon line localized at 18 566 cm^{-1}. The second group of lines is shifted by 302 cm^{-1} from the first group and thus should be assigned as a progression based on the a_{1g} mode. At energies higher than 21 500 cm^{-1} some other groups of low intensity bands are observed (Figure 2, group IV). The vibronic pattern is not clearly resolved, however the progression based on the $\nu_1(a_{1g})$ mode is easily distinguishable.

The energies of the vibronic sidebands assigned for the three lowest energy zero-phonon lines of U^{3+}:Cs_2NaYCl_6, observed in 14 000−17 500 cm^{-1} energy region are given in Table 2.

3.2.2. U^{3+}:Cs_2LiYCl_6. Figure 6 shows a high-resolution absorption spectrum recorded for U^{3+}:Cs_2LiYCl_6 in the $^4I_{9/2} \rightarrow 5f^26d(t_{2g})^1$ transition range. The spectrum consists of four main bands and is similar to that of U^{3+}:Cs_2NaYCl_6. The lowest energy zero-phonon line is localized at 14 296 cm^{-1}. For this line are observed vibronic progressions up to the fourth one, based on the $\nu_1(a_{1g})$ mode of 301 cm^{-1} average energy. The characteristic vibronic pattern is composed of the zero-phonon line and vibronic electric dipole transitions displaced from the zero-phonon line by 55, 109, 159, and 241 cm^{-1} (average values).

The vibronic lines observed in the U^{3+}:Cs_2LiYCl_6 spectrum at energies of 241 and 109 cm^{-1} are assigned as $\nu_2(e_g)$ and $\nu_5(t_{2g})$, respectively. The line at 55 cm^{-1} is assigned as a lattice mode (ν_{LM}). The vibronic line at 159 cm^{-1} (ν_{159}) is most probably the $\nu_{LM} + \nu_5(t_{2g})$ combined band or the $3\nu_{LM}$ band. In group I-B, the next two zero-phonon lines could be easily localized at energies of 15 782 and 16 609 cm^{-1}. The progressions, up to the second one, based on the a_{1g} mode are visible for both lines. The band I-C observed at ∼18 000 cm^{-1} is formed by superimposed vibronic sidebands coupled to the closely positioned zero-phonon lines. The positions of two zero-phonon lines were determined at 17 643 and 17 870 cm^{-1}. In the I-D band with the barycenter at ∼19 900 cm^{-1}, two zero-phonon lines could be localized at energies of 19 327 and 19 837 cm^{-1}. However, in this band the vibronic pattern is not so clearly resolved. The particular lines are broader and the relative

TABLE 2: Positions and Assignments of Vibronic Lines for the First Three of Lowest Energy Zero-Phonon Lines of the $^4I_{9/2} \rightarrow 5f^26d(t_{2g})^1$ Transitions for U^{3+}:Cs_2NaYCl_6 Single Crystal, in the 14 000−17 500 cm^{-1} Energy Range

assignment	line position (cm^{-1})[a]		
zero-phonon	14 158	15 684	16 524
ν_{LM}	45	46	51
ν_{82}	85	82	
ν_5	120		114
ν_{183}	187	181	179
ν_2	226	234	233
ν_1	302	300	302
$\nu_1 + \nu_{LM}$	302 + 42	300 + 47	302 + 51
$\nu_1 + \nu_{82}$	302 + 80		302 + 89
$\nu_1 + \nu_5$		300 + 116	
$\nu_1 + \nu_{183}$	302 + 180	300 + 178	302 + 180
$\nu_1 + \nu_2$	302 + 225	300 + 231	302 + 232
$2\nu_1$	302 + 309 = 611	300 + 304 = 604	302 + 297 = 599
$2\nu_1 + \nu_{LM}$	611 + 41	604 + 50	599 + 52
$2\nu_1 + \nu_5$		604 + 113	
	611 + 147		
$2\nu_1 + \nu_{183}$	611 + 185	604 + 173	
$3\nu_1$	611 + 302 = 913		
$3\nu_1 + \nu_{LM}$	913 + 43		
	913 + 143		
$3\nu_1 + \nu_{183}$	913 + 185		
$4\nu_1$	913 + 301 = 1214		
$4\nu_1 + \nu_{LM}$	1214 + 40		

[a] Except for zero-phonon lines, the values in columns correspond to the energy difference between the zero-phonon line and the vibronic peaks.

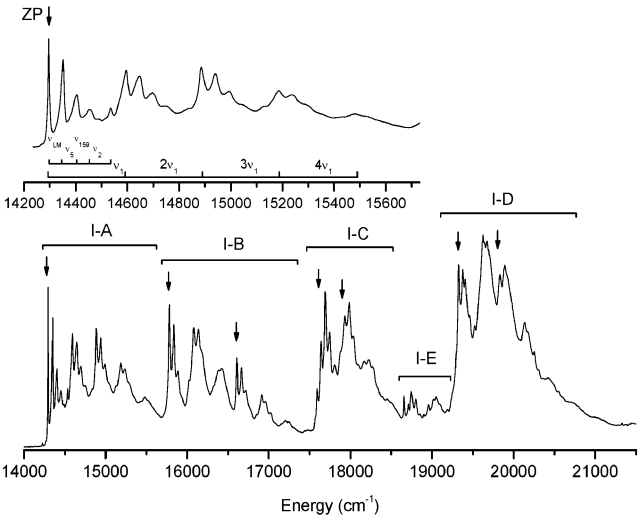

Figure 6. Absorption spectrum recorded at 4.2 K for the U^{3+}:Cs_2LiYCl_6 single crystal in the $^4I_{9/2} \rightarrow 5f^26d(t_{2g})^1$ transition range. The zero-phonon lines are indicated by arrows. In the inset the lowest energy absorption band is presented in extended *x*-axis scale. The vibronic sidebands are shifted by (ν_{LM}) = 55, $\nu_5 = 109$, $\nu_{159} = 159$ and $\nu_2 = 241$ cm^{-1} from the zero-phonon lines. Vibronic progression is seen, which arises from the 301 cm^{-1} totally symmetric $\nu_1(a_{1g})$ stretch of the UCl_6^{3-} moiety.

TABLE 3: Positions and Assignments of Vibronic Lines for the First Three Lowest Energy Zero-Phonon Lines of the $^4I_{9/2} \rightarrow 5f^26d(t_{2g})^1$ Transitions for U^{3+}:Cs_2LiYCl_6 Crystal in the 14 000−17 500 cm^{-1} Energy Range

assignment	line position (cm^{-1})[a]		
zero-phonon	14 296	15 782	16 609
ν_{LM}	55	56	58
ν_5	109	106	111
ν_{159}	159	159	
ν_2	245	243	242
ν_1	300	298	301
$\nu_1 + \nu_{LM}$	300 + 54	298 + 56	301 + 51
$\nu_1 + \nu_5$	300 + 106	298 + 102	301 + 108
$\nu_1 + \nu_{159}$	300 + 153		
$\nu_1 + \nu_2$	300 + 245	298 + 237	301 + 243
$2\nu_1$	300 + 293 = 593	298 + 297 = 595	301 + 294 = 595
$2\nu_1 + \nu_{LM}$	593 + 55	595 + 48	599 + 48
$2\nu_1 + \nu_5$	593 + 109		
$2\nu_1 + \nu_{159}$	593 + 156		
$2\nu_1 + \nu_2$	593 + 247		
$3\nu_1$	593 + 297 = 890		
$3\nu_1 + \nu_{LM}$	890 + 52		
$3\nu_1 + \nu_5$	890 + 105		
$3\nu_1 + \nu_{159}$	890 + 161		
$3\nu_1 + \nu_2$	890 + 242		
$4\nu_1$	890 + 294 = 1184		
$4\nu_1 + \nu_{LM}$	1214 + 51		

[a] Except for zero-phonon lines, the values in columns correspond to the energy difference between the zero-phonon line and the vibronic peaks.

intensity of this band is larger as compared to lower energy bands. This may suggest that in this band the vibronic sidebands coupled with the two mentioned above zero-phonon lines are superimposed with other sidebands connected with unidentified zero-phonon lines. Besides, the (I-E) group of lines of lower intensity but with a well-resolved fine structure is observed between the bands I-C and I-D at ∼18 850 cm^{-1}. The first band of this group is composed of vibronic electric dipole transitions coupled to the zero-phonon line localized at 18 657 cm^{-1}. The displacement of the vibronic lines from the zero-phonon line is the same as observed for the more intense bands. The second group of lines is shifted by 300 cm^{-1} from the first group and thus should be assigned as the first progression of the a_{1g} mode based on the zero-phonon line at 18 657 cm^{-1}. Another group of low intensity bands (group IV in Figure 2) is similar to those for the Cs_2NaYCl_6 host crystal, observed at energies higher than 21 000 cm^{-1}.

The energies of the vibronic sidebands assigned for the three lowest energy zero-phonon lines of U^{3+}:Cs_2LiYCl_6 observed in the 14 000−17 500 cm^{-1} energy region are given in Table 3.

3.2.3. U^{3+}:Cs_2NaYBr_6. Figure 7 presents in details the absorption spectrum of U^{3+}:Cs_2NaYBr_6 in the $^4I_{9/2} \rightarrow 5f^26d(t_{2g})^1$ transition range. In this spectrum, in contrast to those of U^{3+}:Cs_2NaYCl_6 and U^{3+}:Cs_2LiYCl_6, one does not observe a fine structure arising from vibronic electric dipole transitions assigned as $\nu_2(e_g)$, $\nu_5(t_{2g})$, and lattice modes (ν_{LM}) but only the vibronic progression based on the $\nu_1(a_{1g})$ stretch. It results from a cubic-to-tetragonal phase transition occurring during the cooling of the U^{3+}:Cs_2NaYBr_6 crystal from room to helium temperatures.[44,34] As a consequence, the details of the spectrum are lost and only some approximate positions of the zero-phonon lines could be deduced from the observed $\nu_1(a_{1g})$ progression.

The energy of the $\nu_1(a_{1g})$ stretching mode of Cs_2NaYBr_6:U^{3+} was determined from Raman spectra at 177 cm^{-1} (ref 45). The I-A group is formed by seven bands. The first broad and unstructured maximum is formed by the zero-phonon line

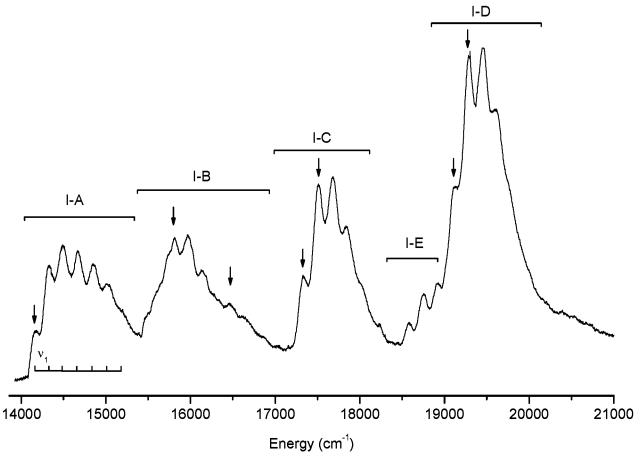

Figure 7. Absorption spectrum recorded at 4.2 K for the U^{3+}:Cs_2NaYBr_6 single crystal in the $^4I_{9/2} \rightarrow 5f^26d(t_{2g})^1$ transition range. The zero-phonon lines are indicated by arrows. Vibronic progression is seen, based on a ∼180 cm^{-1} totally symmetric $\nu_1(a_{1g})$ stretch of the UBr_6^{3-} moiety.

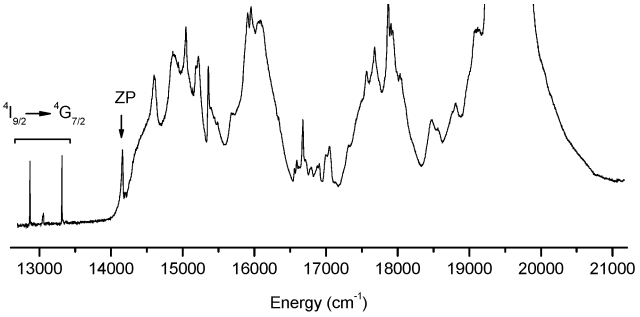

Figure 8. Absorption spectrum recorded at 4.2 K for the U^{3+}:$CsCdBr_3$ single crystal in the $^4I_{9/2} \rightarrow 5f^26d(t_{2g})^1$ transition range. The $5f^3 \rightarrow 5f^3$ ($^4I_{9/2} \rightarrow {}^4G_{7/2}$) transitions are observed at ∼13 000 cm^{-1}. The lowest energy $^4I_{9/2} \rightarrow 5f^26d(t_{2g})^1$ zero-phonon line is marked with an arrow.

located at ∼14 134 cm^{-1}, followed by unresolved vibronic sidebands due to $\nu_2(e_g)$, $\nu_5(t_{2g})$ and lattice mode (ν_{LM}) vibrations. The distance between subsequent maxima is between ∼160 and 185 cm^{-1}, which suggest that these are subsequent steps of the $\nu_1(a_{1g})$ vibronic progression. In the next group (I-B), two zero-phonon lines could be assigned at 15 795 and 16 455 cm^{-1}. In the group I-C, the zero-phonon lines are located at 17 330 and 17 500 cm^{-1}, while in the band I-D they are placed at 19 105 and 19 280 cm^{-1}. Between the groups I-C and I-D three bands of lower intensity are also observed. They are spaced by ∼170 cm^{-1}, which suggest that the first band is composed of vibronic transitions coupled to the zero-phonon line at ∼18 540 cm^{-1}, and the two other bands are the first and second vibronic progression of the $\nu_1(a_{1g})$ stretch. Low intensity bands are observed also at energies higher than 21 000 cm^{-1}.

3.2.4. U^{3+}:$CsCdBr_3$ and U^{3+}:$Cs_3Lu_2Cl_9$. The main features of the U^{3+}:$CsCdBr_3$ spectrum shown in Figure 8 are similar to that of U^{3+}:Cs_2NaYBr_6 (Figure 7). However, the fine structure is more complicated, and a detailed assignment is not possible. This results mainly from the lower symmetry (C_{3v}) of U^{3+} ions in $CsCdBr_3$, which leads to the splitting of the $5f^26d^1$ configuration into a larger number of CF levels than that for the O_h symmetry. Moreover the difference in relative intensities between the $5f^3 \rightarrow 5f^26d^1$ and $5f^3 \rightarrow 5f^3$ transitions (see, e.g., the $^4I_{9/2} \rightarrow {}^4G_{7/2}$ transitions shown in Figure 8) is smaller than those in elpasolite host crystals with a pure O_h symmetry. Hence, the $5f^3 \rightarrow 5f^3$ transitions, superimposed on the vibronic structure of the $5f^3 \rightarrow 5f^26d^1$ bands could be observed in the investigated

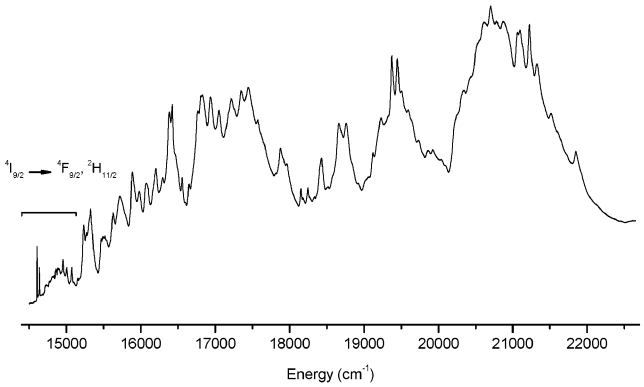

Figure 9. Absorption spectrum recorded at 4.2 K for the U^{3+}:$Cs_3Lu_2Cl_9$ single crystal in the $^4I_{9/2} \rightarrow 5f^26d(t_{2g})^1$ transition range. The sharp lines observed at the lowest energy region are due to $5f^3 \rightarrow 5f^3$ ($^4I_{9/2} \rightarrow {}^4F_{9/2}$, $^2H_{11/2}$) transitions.

spectral region, making the assignment very difficult. Nevertheless, the four main bands with barycenters at ∼14 800, 16 000, 17 800, and 19 700 cm^{-1} could be distinguished. The positions and shapes of these bands are similar to those in the U^{3+}:Cs_2NaYBr_6 spectrum which suggests, that for the $CsCdBr_3$ crystal octahedral part of crystal-field dominates and trigonal part is smaller distortion. The relatively sharp peak observed at 14 159 cm^{-1} has been assigned as the lowest energy $5f^3 \rightarrow 5f^56d^1$ transition, and its energy is almost the same as the energy of the first zero-phonon transition of U^{3+} in Cs_2NaYBr_6.

The structure of the U^{3+}:$Cs_3Lu_2Cl_9$ spectrum (Figure 9) is significantly different from that of U^{3+}:Cs_2NaYCl_6. The trigonal distortion is more significant and cannot be treated as a small one as compared to the octahedral part of the crystal-field. This leads to a father splitting of the $5f^26d^1$ configuration into a larger number of crystal-field levels than for crystals with pure O_h symmetry. Moreover, one may observe relatively strong $5f^3 \rightarrow 5f^3$ transitions, which may overlap with those of $5f^3 \rightarrow 5f^26d^1$. As a consequence, in the U^{3+}:$Cs_3Lu_2Cl_9$ spectrum none of the zero-phonon lines could be unambiguously identified.

4. Discussion

4.1. Uranium (4+). In contrast to the corresponding absorption spectra of the U^{3+} ion (see group I in Figure 2) we have not notice any significant changes in the feature of the U^{4+} absorption spectra (group II) when the site symmetry of the central metal ion lowers from O_h (e.g., in U^{4+}:Cs_2NaYCl_6:) to C_{3v} (U^{4+}:$Cs_3Lu_2Cl_9$:). In the case of U^{3+} dopant ions the substitution for Y^{3+} or Lu^{3+} does not require any charge compensation and the site symmetry of the central ion (O_h for elpasolites or C_{3v} for $Cs_3Lu_2Cl_9$) is retained. One may expect, however, that the substitution of trivalent ions by U^{4+} ions will require some charge compensation. In the elpasolites the site symmetry of the U^{4+} dopant is lower than O_h, and that of C_{3v} in $Cs_3Lu_2Cl_9$ is probably also disturbed. Thus, since it is also disturbed, the site symmetry of U^{4+} may be not very sensitive to a small trigonal distortion and a lowering of the nominal site symmetry from O_h to C_{3v}.

So far, to the best of our knowledge, an analysis of $5f^2 \rightarrow 5f^16d^1$ transitions for U^{4+} ions doped in chloride or bromide host crystals have not been reported. For the isoelectronic $4f^2$ Pr^{3+} ion doped in Cs_2NaYCl_6 single crystals the energy of the lowest $4f^16d^1$ electronic level was recorded at 39 017 cm^{-1} (ref 46). For U^{4+} ions doped in these crystals the first $5f^2 \rightarrow 5f^16d^1$ transition is observed at about 8000 cm^{-1} lower energy i.e., at ∼31 000 cm^{-1}. This value is comparable with the ∼8200 cm^1 difference between the lowest f−d electronic level in the isoelectronic $4f^1$ Ce^{3+}:Cs_2NaYCl_6 (ref 52) and $5f^1$ Pa^{4+}:Cs_2NaYCl_6 (refs 23 and 24) crystals. For the U^{3+}- and U^{4+}-doped Cs_2NaYCl_6 crystals the f−d transitions of lowest energy are observed at 14 158 and ∼31 010 cm^{-1}, respectively. For comparison, in the absorption spectrum of U^{4+}:$LiYF_4$ single crystals the first f−d transitions are observed at ∼40 000 cm^{-1} (refs 27 and 28), while those for U^{3+}:$LiYF_4$ appear at ∼20 000 cm^{-1} (ref 13). Thus, in both of these crystals the U^{3+} f−d transitions are positioned at an energy of ∼50% lower than those of U^{4+}. Ab initio theoretical studies[47] have predicted the energies of the crystal field levels in 31 100−51 000 cm^{-1} spectral range for the $5f^16d(t_{2g})^1$ manifold of U^{4+} ions doped in Cs_2ZrCl_6 crystals, in which the uranium ions possess a similar environment with that in Cs_2NaYCl_6. The first three symmetry allowed zero-phonon transitions calculated at energies of 32 500, 33 900, and 35 800 cm^{-1} correspond very well with those of U^{4+} doped in the chloride host crystals presented in this paper. Since the following transitions to the $5f^16d(e_g)^1$ manifold are obscured by strong bands of the edge of lattice absorption they could not be observed. The predicted energies of these transitions for U^{4+}:Cs_2ZrCl_6 amounts to 67 300−85 500 cm $^{-1}$ (ref 47). Hence, similar values should be expected also for U^{4+} ions in the investigated crystals.

4.2. Uranium(3+). The ground state of the $5f^3$ configuration in a crystal-field of O_h symmetry is Γ_{8u} ($^4I_{9/2}$). The crystal field splits the $6d^1$ electronic state into a t_{2g} lower and e_g upper state. The $6d^1$ spin−orbit coupling, which is much smaller than the CF affecting 6d electrons, removes the triply degeneracy of t_{2g} and splits this level into a Γ_{8g} degenerate quartet and a higher lying Γ_{7g} Kramer's doublet. For the $5f^26d^1$ excited configuration the energy level structure is far more complicated. A simplified diagram showing the $5f^26d^1$ energy levels structure is shown in Figure 10. The coupling of the split by the crystal-field and spin−orbit interactions 6d state with the $5f^2$ core electrons leads to a number of following levels. Those with the lowest energy result from interaction of the $6d(t_{2g})\Gamma_{8g}$ state with the $5f^2(^3H_4)$ and can be described as $5f^2(^3H_4)-6d(t_{2g})^1(\Gamma_{8g})$. The next group of states, at higher energies should then arise from the $5f^2(^3H_4)-6d(t_{2g})^1(\Gamma_{7g})$ configuration. The energy difference between the Γ_{8g} and Γ_{7g} states (i.e., the splitting of the t_{2g} state) resulting from spin−orbit interaction of the 6d electron can be conveniently observed in spectra of ions with a $6d^1$ excited configuration, e.g., for Pa^{4+}:Cs_2ZrCl_6 the splitting of the t_{2g} state amounts to 3046 cm^{-1} (ref 24). Assuming that the spin−orbit constant of 6d electrons has a similar value as well for protactinium and uranium ions one expect that the splitting of the t_{2g} state for U^{3+} is at least equal to 3000 cm^{-1}.

In the investigated spectra of U^{3+} ions with an O_h site symmetry are observed four main bands in the 14 000−21 000 cm^{-1} range (Figures 5−7). The 1400 cm^{-1} distance between bands I-A and I-B corresponds to that observed between bands I-C and I-D, which is equal to 1600 cm^{-1}, and that between bands I-A and I-C as well as that between I-B and I-D is close to 3350 cm^{-1}. Thus, it seems that the first two bands (I-A and I-B) are formed by lines due to transitions to crystal-field levels arising from the $5f^2(^3H_4)-6d(t_{2g})^1(\Gamma_{8g})$ configuration, while the two bands of higher energy (I-C and I-D) are due to transitions to levels originating from the $5f^2(^3H_4)-6d(t_{2g})^1(\Gamma_{7g})$ configuration. The lower intensity band I-E, observed at ∼18 800 cm^{-1} is shifted from the band I-A by ∼4500 cm^{-1}. For the $5f^2$ configuration of U^{4+} ions doped in the Cs_2ZrCl_6 crystal, where they occupy a site of O_h symmetry, the first excited $^3F_2$ multiplet was observed at 5500 cm^{-1} (ref 48). Thus, the band I-E arises

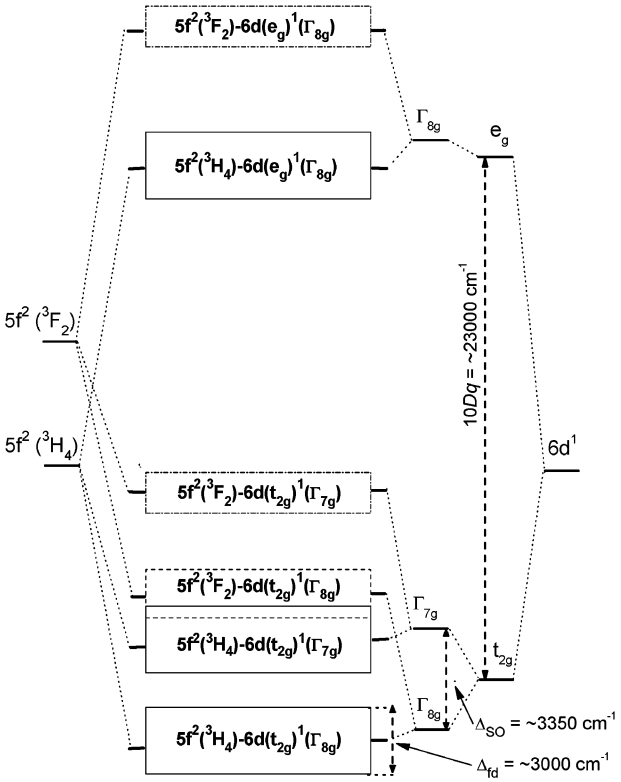

Figure 10. Schematic diagram showing energy levels originating from $5f^26d^1$ configuration of U^{3+} in UCl_6^{3-} complexes. The experimental splitting due to the crystal field interaction ($10Dq$) and spin−orbit coupling of 6d electron (Δ_{SO}) and the splitting (Δ_{fd}) of $5f^2(^{2S+1}L_J)-6d(\gamma)^1(\Gamma_{ig})$ ($\gamma = t_{2g}$ or e_g) configurations arising from coupling of $5f^2$ core electrons and 6d electron are shown (numerical values are given for U^{3+} in Cs_2NaYCl_6 crystal).

from transitions to the $5f^2(^3F_2)-6d(t_{2g})^1(\Gamma_{8g})$ configuration. Transitions to configurations in which two 5f electrons are in excited state are expected to be of low intensity, since only the second-order terms contribute to the electric dipole moments. The next group of relatively weak lines is observed at ∼22 000 cm^{-1} (group IV in Figure 2), which is ∼3200 cm^{-1} above band I-E, and consequently should be assigned as transitions to the $5f^2(^3F_2)-6d(t_{2g})^1(\Gamma_{7g})$ configuration.

A somewhat different assignment of the observed bands has been proposed by Seijo et al.[40] Similarly as in the present paper the most intense bands I-A, I-B, I-C, and I-D have been assigned as transitions to the $5f^2(^3H_4)-6d(t_{2g})^1$ configuration. However, on the basis of ab initio calculations the Authors have suggested, that the I-A, I-B, and I-C bands should be assigned as transitions to the $5f^2(^3H_4)-6d(t_{2g})^1(\Gamma_{8g})$ configuration, while only last I-D band to the $5f^2(^3H_4)-6d(t_{2g})^1(\Gamma_{7g})$ configuration. Since both of these configurations results from a coupling with the $5f^2(^3H_4)$ state, they should exhibit a similar magnitude of the CF splitting. Thus, we have assumed that the I-A and I-B bands are due to transitions to levels resulting from the $5f^2(^3H_4)-6d(t_{2g})^1(\Gamma_{8g})$ configuration, while those of I-C and I-D to levels resulting from the $5f^2(^3H_4)-6d(t_{2g})^1(\Gamma_{7g})$ configuration. Hence, in our assignment the CF splitting is equal to ∼3000 cm^{-1} for both configurations, whereas from the calculations of Seijo and Barandiaran results in the values of ∼3700 and ∼1000 cm^{-1} for $5f^2(^3H_4)-6d(t_{2g})^1(\Gamma_{8g})$ and $5f^2(^3H_4)-6d(t_{2g})^1(\Gamma_{7g})$, respectively.

An other discrepancy concerns the $5f^2(^3F_2)-6d(t_{2g})^1(\Gamma_{8g})$ and $5f^2(^3F_2)-6d(t_{2g})^1(\Gamma_{8g})$ levels. From ab initio calculations results in that levels with a main character $5f^2$(other than $^3H_4$) × $6d(t_{2g})^1$ should be observed as low intensity bands at energies higher than 20 480 cm^{-1}. Such transitions are indeed experimentally observed at wavenumbers >21 000 cm^{-1} (bands IV in Figure 2). However, in our spectra a similar group of low intensity bands has been observed also in the 18 500−19 100 cm^{-1} range (bands I-E in Figure 5), whereas the calculations presented by Seijo and Barandiaran does not predict the appearance of any energy levels in this region. Since the 3350 cm^{-1} energy distance between I-E and IV group of bands approximately corresponds to the splitting resulting from the spin−orbit coupling (Δ_{SO}), we have assigned the I-E and IV bans as transitions to the $5f^2(^3F_2)-6d(t_{2g})^1(\Gamma_{8g})$ and $5f^2(^3F_2)-6d(t_{2g})^1(\Gamma_{7g})$ configurations, respectively.

It seems that some other calculations would be required in order to prove which of the proposed assignments is correct, especially when one take into account that the differences (seen in energy units) are relatively small, equal to ∼2000 cm^{-1}, which may be within the limit of accuracy of the ab initio method. For example, as will be shown in the subsequent part of this paper, the lowest level of the $5f^26d(e_g)^1$ configuration is for U^{3+}:Cs_2NaYCl_6 observed at ∼40 700 cm^{-1}, while the ab initio calculations predict its location above 42 000 cm^{-1}. One may consider it as a pretty good agreement, but nevertheless, the absolute difference amounts to about 1300 cm^{-1}.

Transitions to the $5f^26d(e_g)^1$ levels of the U^{3+} ion could not be analyzed in detail. They appear as broad and unstructured bands at wavenumbers higher than 38 000 cm^{-1}. The absence of a fine structure in the transitions to higher-energy $4f^{N-1}5d$ states has been observed also for lanthanide ions[49] and was explained by assuming that these high-energy levels are positioned in the conduction band of the host lattice. Fast photoionization processes lead to a reduction of excited-state lifetimes and as result of these to a considerable line broadening.

In the spectrum of U^{3+}:Cs_2NaYCl_6 such a broad band was observed at ∼40 700 cm^{-1} and a less intense at ∼44 400 cm^{-1} (Figure 2). The e_g level is not split by spin−orbit interactions and transforms in the O_h symmetry as Γ_{8g}. Thus, band IIIA is composed of transitions to crystal-field levels, which can be described as $5f^2(^3H_4)-6d(e_g)^1(\Gamma_{8g})$. The lower intensity band is located at ∼3700 cm^{-1} higher energy, which corresponds to the energy difference between the $^3H_4$ and $^3F_2$ states of the $5f^2$ core electrons. Hence, the lower intensity band may be assigned as $5f^2(^3F_2)-6d(e_g)^1(\Gamma_{8g})$. The observed bands corresponds well with the results of ab initio calculations,[40] which have predicted the appearance of bands of the $5f^26d(e_g)^1$ configuration at wavenumbers above 42 000 cm^{-1}.

For U^{3+}:Cs_2LiYCl_6 the transitions to the $5f^2(^3H_4)-6d(e_g)^1(\Gamma_{8g})$ levels arise as a broad band with two maxima at 39 750 and 41100 cm^{-1} (Figure 2b). The distance of 1350 cm^{-1} between these two maxima corresponds to the extent of the $5f^2(^3H_4)-6d(t_{2g})^1(\Gamma_{8g})$ configuration. The lower intensity transitions to the $5f^2(^3F_2)-6d(e_g)^1(\Gamma_{8g})$ configuration are observed at ∼43 400 cm^{-1}. For U^{3+}:Cs_2NaYBr_6, transitions to the e_g levels are weak; nevertheless, two maxima may be distinguished at ∼37 000 and 40 300 cm^{-1} (Figure 2c).

The determined energy levels for $5f^26d^1$ configuration of U^{3+}-doped elpasolite crystals are given in Table 4.

The first f−d transitions are for U^{3+} ions observed at a significantly lower energy than for Nd^{3+} ions. For example for Nd^{3+}:Cs_2NaYCl_6 the first $4f^3 \rightarrow 4f^25d^1$ absorption maximum is observed around 47 600 cm^{-1} (ref 50), that is at a 33 400 cm^{-1} higher energy than for U^{3+} in the same host crystal. The positions of the first f−d transitions in the chloride hosts crystals are also lower than for the fluorides, where they appear at 20 000

TABLE 4: Energy Levels of the $5f^26d^1$ Configuration of U^{3+} Ions Doped in Cs_2NaYCl_6, Cs_2LiYCl_6, and Cs_2NaYBr_6 Single Crystals

	compound		
manifold	Cs_2NaYCl_6	Cs_2LiYCl_6	Cs_2NaYBr_6
$5f^5(^3H_4)-6d(t_{2g})^1(\Gamma_{8g})$	14 158	14 296	14 134
	15 684	15 782	15 795
	16 524	16 609	16 455
$5f^5(^3H_4)-6d(t_{2g})^1(\Gamma_{7g})$	17 597	17 643	17 330
	17 774	17 870	17 500
	19 250	19 327	19 105
	19 544		19 280
	19 568		
	19 740	19 837	
$5f^5(^3F_2)-6d(t_{2g})^1(\Gamma_{8g})$	18 566	18 657	18 540
$5f^5(^3H_4)-6d(e_g)^1(\Gamma_{8g})$	40 700	39 750	37 000
		41 100	
$5f^5(^3F_2)-6d(e_g)^1(\Gamma_{8g})$	44 400	43 400	40 300

and 25 000 cm^{-1} for U^{3+} in $LiYF_4$ (ref 13) and UF_3 (ref 51), respectively.

For U^{3+}:Cs_2NaYCl_6 the $5f^2(^3H_4)-6d(e_g)^1(\Gamma_{8g})$ levels are positioned at ∼40 700 cm^{-1}. The barycenter of the $5f^2(^3H_4)-6d(t_{2g})^1$ levels is at ∼17 700 cm^{-1}. Thus, the crystal field splitting (10*Dq*) of the $5f^26d^1$ configuration of U^{3+} ions is equal to ∼23 000 cm^{-1}. As one could expect, it is somewhat larger than the 20 000 cm^{-1} value determined for Ce^{3+}:Cs_2NaYCl_6 (ref 52). For U^{4+} ions a stronger crystal field effect is expected, but unfortunately any experimental 10*Dq* values are not available. Ab initio calculations performed for U^{4+}-doped Cs_2ZrCl_6 single crystals show that the crystal levels of the $5f^26d(t_{2g})^1$ and $5f^26d(e_{2g})^1$ manifolds should arise in the in the 31 100−51 000 and 67 300−85 500 cm^{-1} range, respectively,[47] from which results a 10*Dq* value of ∼35 000 cm^{-1}. For Pa^{4+} ions the reported experimental value of 10*Dq* amounts to ∼18 600 cm^{-1} (ref 23), which seems to be too low as compared to that of Ce^{3+} ions, since the extension of the 6d orbitals is larger than that of 5d. However, from the ab inition calculations performed by Seijo et al.,[25] a considerably larger value of ∼30 000 cm^{-1} resulted for the 10*Dq* parameter of Pa^{4+} in Cs_2ZrCl_6. Thus, the theoretically calculated 10*Dq* values for U^{4+} and Pa^{4+} ions correspond well to that of U^{3+} determined in these investigations.

For U^{3+}:Cs_2LiYCl_6 the $5f^2(^3H_4)-6d(e_g)^1(\Gamma_{8g})$ levels are observed at ∼39 750 cm^{-1}. The barycenter of the $5f^2(^3H_4)-6d(t_{2g})^1$ levels is at about 17 000 cm^{-1}. Thus, the CF splitting (10*Dq*) of the $5f^26d^1$ configuration is equal to ∼22 750 cm^{-1} and is smaller than for the U^{3+}:Cs_2NaYCl_6 crystal. The same relation was observed for the splitting of the L′S′J′ multiplets of the $5f^3$ configuration which results from somewhat shorter Y−Cl distances in Cs_2LiYCl_6 crystals. A still weaker CF is expected for the bromide elpasolites and indeed, the first transitions to the $5f^2(^3H_4)-6d(e_g)^1(\Gamma_{8g})$ levels were observed at ∼36 700 cm^{-1}, which determine a ∼19 700 cm^{-1} crystal-field splitting (10*Dq*).

Certainly, the energy levels of the $5f^26d^1$ excited configuration cannot be properly reproduced by limiting the analysis to the splitting of the $5f^2$ core levels, superimposed on the split 6d state. However, the splitting of the $5f^2(^{2S+1}L_J)-6d(\gamma)^1(\Gamma_{ig})$ ($\gamma = t_{2g}$ or e_g) manifolds resulting from the coupling of the $5f^2$ core electrons and the 6d electron is smaller than the splitting between the $5f^2(^{2S+1}L_J)-6d(\gamma)^1(\Gamma_{8g})$ and $5f^2(^{2S+1}L_J)-6d(\gamma)^1(\Gamma_{7g})$ configurations resulting from the spin−orbit coupling of 6d electrons (see Figure 10). Thus, the main feature of the observed crystal level structure reflects the dominating influence of the CF splitting and spin−orbit coupling of the 6d electron. These interactions split the $5f^26d^1$ configuration into groups of energy levels. Transitions to these groups are labeled as I-A, ..., I-E in Figure 2. Each particular group consist of a number of energy levels due to interactions within the $5f^26d^1$ configuration. For the description of the energy levels structure within such groups, the Coulomb interactions between the 5f electrons and the 6d electron should be at least included.

5. Summary

Absorption spectra of U^{3+}-doped Cs_2NaYCl_6, Cs_2LiYCl_6, Cs_2NaYBr_6, $CsCdBr_3$, and $Cs_3Lu_2Cl_9$ single crystals were recorded at 4.2 K in the 14 000−50 000 cm^{-1} energy range. The common feature of all investigated host lattices are MX_6^{3-} octahedra. In the elpasolites U^{3+} ions substitute for Y^{3+} in a site of O_h symmetry, while in the $CsCdBr_3$ and $Cs_3Lu_2Cl_9$ crystals the metal site symmetry is C_{3v}, but the crystal-field at the impurity ion can be described as the superposition of a dominant octahedral and a weaker trigonal one.

In all investigated spectra were observed f−d transitions of U^{4+} impurities in the 30 000−37 000 cm^{-1} energy range. They have been assigned as transitions from the lowest crystal field component of the $^3H_4$ ground multiplet of the $5f^2$ configuration to energy levels of the $5f^16d(t_{2g})^1$ manifold. The lowest energy level of this manifold has been found at 26 360 and 28 590 cm^{-1} for U^{4+}:$CsCdBr_3$ and U^{4+}:Cs_2NaYBr_6, respectively. In the chloride host crystals this level is placed in the 30 360−31 010 cm^{-1} energy range. It is positioned in the U^{4+}:Cs_2NaYCl_6 crystals at an energy of ∼8000 cm^{-1} lower than for the isoelectronic Pr^{3+} ion and of ∼16 000 cm^{-1} higher than for U^{3+} ions in the same host. To the best of our knowledge, for the first time these levels have been determined for U^{4+} ions doped in a chloride or bromide host crystal and so far has been established for U^{4+}-doped $LiYF_4$ crystals only.[26,27]

For U^{3+} ions the transitions from the $^4I_{9/2}$ ground level to $5f^26d(t_{2g})^1$ crystal field levels are observed in the 4000−21 000 cm^{-1} range as fine structured broad bands. The most prominent feature of the spectra is the vibronic a_{1g} progression built on each of the zero-phonon lines. Superimposed on these progression are farther vibronic electric dipole transitions corresponding to even parity vibrations of the $M(U)Cl_6^{3-}$ complex or to host lattice modes. The number of zero-phonon lines have been identified. They have been assigned as transitions to crystal-field levels arising from the $5f^2(^3H_4)-6d(t_{2g})^1(\Gamma_{8g})$ (barycenter at ∼16 000 cm^{-1}) and $5f^2(^3H_4)-6d(t_{2g})^1(\Gamma_{7g})$ (barycenter at ∼19 000 cm^{-1}) configurations. Besides, the low intensity bands observed at ∼18 600 cm^1 and above 21 000 cm^{-1} have been assigned as transitions to energy levels of the $5f^2(^3F_2)-6d(t_{2g})^1(\Gamma_{8g})$ and $5f^2(^3F_2)-6d(t_{2g})^1(\Gamma_{7g})$ configurations, respectively. The resulting from spin−orbit interaction difference between the Γ_{8g} and Γ_{7g} states in U^{3+}:Cs_2NaYCl_6 has been for the 6d electron evaluated at 3350 cm^{-1}. The lowest energy level of the $5f^2(^3H_4)-6d(t_{2g})^1(\Gamma_{8g})$ configuration is observed for U^{3+} doped in Cs_2LiYCl_6 and Cs_2NaYCl_6 at 14 296 and 14 158 cm^{-1}, respectively and at only slightly lower energy of 14 134 cm^{-1} for U^{3+}:Cs_2NaYBr_6. The position of the first f−d transitions of U^{3+} ions is observed at a 33 400 cm^{-1} lower energy than that of the isoelectronic Nd^{3+} ions in the same crystal.

Transitions to the e_g levels of U^{3+} ions are observed as broad and unstructured bands at wavenumbers higher than 38 000 cm^{-1}. The crystal field splitting (10*Dq*) of the $5f^26d^1$ configuration of U^{3+} doped in Cs_2NaYCl_6 is about 23 000 cm^{-1}, and that in Cs_2NaYBr_6 amounts to ∼19 700 cm^{-1}.

The splitting of the $5f^2(^{2S+1}L_J)-6d(\gamma)^1(\Gamma_{ig})$ ($\gamma = t_{2g}$ or e_g) configuration resulting from the coupling of the $5f^2$ core

electrons and 6d electron is equal to ~3000 cm^{-1} and is smaller than the ~3350 cm^{-1} splitting between the $5f^2(^{2S+1}L_J)-6d(\gamma)^1(\Gamma_{8g})$ and $5f^5(^{2S+1}L_J)-6d(\gamma)^1(\Gamma_{7g})$ configurations resulting from the spin−orbit coupling of the 6d electron. Hence, the main feature of the crystal level structure observed in absorption spectra reflects the dominating influence of the CF splitting and spin−orbit coupling of the 6d electron. The tabulated energy levels should have essential importance for more sophisticated theoretical analyses such as that presented for Pa^{4+} and U^{4+} in Cs_2ZrCl_6 (refs 25 and 47).

Acknowledgment. This work was supported by the Polish Committee for Scientific Research within the Project No. 7TO9A080 20, which is gratefully acknowledged.

References and Notes

(1) Karbowiak, M.; Drożdżyński, J.; Murdoch, K. M.; Edelstein, N. M.; Hubert, S. *J. Chem. Phys.* **1997**, *106*, 3067.
(2) Karbowiak, M.; Edelstein, N. M.; Gajek, Z.; Drożdżyński, J. *Spectrochim. Acta A* **1998**, *54*, 2035.
(3) Karbowiak, M.; Drożdżyński, J.; Hubert, S.; Simoni, E.; Stręk, W. *J. Chem. Phys.* **1998**, *108*, 10181.
(4) Karbowiak, M.; Drożdżyński, J.; Sobczyk, M. *J. Chem. Phys.* **2002**, *117*, 2800.
(5) Karbowiak, M.; Mech, A.; Drożdżyński, J.; Gajek, Z.; Edelstein, N. M. *New J. Chem.* **2002**, *26*, 1651.
(6) Karbowiak, M.; Drożdżyński, J. *J. Alloys Compd.* **2000**, *300−301*, 329.
(7) Karbowiak, M.; Gajek, Z.; Drożdżyński, J. *Chem. Phys.* **2000**, *261*, 301.
(8) Karbowiak, M.; Drożdżyński, J.; Gajek, Z. *J. Alloys Compd.* **2001**, *323−324*, 678.
(9) Wybourne, B. G. *Spectroscopic Properties of Rare Earths;* Interscience: New York, 1965.
(10) Mulak, J.; Gajek, Z. *The Effective Crystal Field Potentia;* Elsevier: Amsterdam, 2002.
(11) Carnall, W. T. *ANL-89/39 report;* Argonne National Laboratory, Chicago, IL, 1989.
(12) Sobczyk, M.; Karbowiak, M.; Drożdżyński, J. *J. Solid State Chem.* **2003**, *170*, 443.
(13) Simoni, E.; Louis, M.; Gesland, J. Y.; Hubert, S. *J. Lumin.* **1995**, *65*, 153.
(14) Sytsma, J.; Piehler, D.; Edelstein, N. M.; Boatner, L. A.; Abraham, M. M. *Phys. Rev. B* **1993**, *47*, 14786.
(15) Marsman, M.; Andriessen, J.; van Eijk, C. W. E. *Phys. Rev. B* **2000**, *61*, 16477.
(16) Chase, L. L. *Phys. Rev. B* **1970**, *2*, 2308.
(17) Weakliem, H. A. *Phys. Rev. B* **1972**, *6*, 2743.
(18) Johnson, K. E.; Sandoe, J. N. *J. Chem. Soc. A* **1969**, 1694.
(19) Meijerink, A.; Wegh, R. T.; van Pieterson, L. *Proc. Electrochem. Soc.* **2000**, *99−40*, 23.
(20) Reid, M. F.; van Pieterson, L.; Wegh, R. T.; Meijerink, A. *Phys. Rev. B* **2000**, *62*, 14744.
(21) van Pieterson, L.; Reid, M. F.; Wegh, R. T.; Soverna, S.; Meijerink, A. *Phys. Rev. B* **2002**, *65*, 045113.
(22) van Pieterson, L.; Reid, M. F.; Burdick, G. W.; Meijerink, A. *Phys. Rev. B* **2002**, *65*, 045114.
(23) Edelstein, N.; Kot, W. K.; Krupa, J.-C. *J. Chem. Phys.* **1992**, *96*, 1.
(24) Piehler, D.; Kot, W. K.; N. Edelstein, N. *J. Chem. Phys.* **1991**, *94*, 942.
(25) Seijo, L.; Barandiaran, Z. *J. Chem. Phys.* **2001**, *115*, 5554.
(26) Naik, R. C.; Krupa, J. C. *J. Lumin.* **1984**, *31/32*, 222.
(27) Godbole, S. V.; Page, A. G.; Sangeeta; Sabharwal, S. C.; Gesland, J. Y.; Sastry, M. D. *J. Lumin.* **2001**, *93*, 213.
(28) Kirikowa, N. Yu.; Kirm, M.; Krupa, J. C.; Makhov, V. N.; Zimmer, G.; Gesland, J. Y. *J. Lumin.* **2002**, *97*, 174.
(29) Kaminskaya, A. N.; Drożdżyński, J.; Mikheev, N. B. *Radiokhimiya* **1980**, *22*, 247.
(30) Kaminskaya, A. N.; Drożdżyński, J.; Mikheev, N. B. *Radiokhimiya* **1981**, *23*, 264.
(31) Mazurak, Z.; Drożdżyński, J.; Hanuza, J. *J. Mol. Struct.* **1988**, *171*, 443.
(32) Drożdżyński, J. *Acta Phys. Pol., A* **1993**, *84*, 975.
(33) Dereń, P. J.; Strek, W.; Drożdżyński, J. *J. Appl. Spectrosc.* **1995**, *62*, 58.
(34) Karbowiak, M.; Drożdżyński, J.; Zych, E.; Dereń, P. *Chem. Phys.* **2003**, *287*, 365.
(35) McPherson, G. L.; McPherson, A. M.; Atwood, J. L. *J. Chem. Phys. Solids* **1980**, *41*, 495.
(36) Henling, L. M.; McPherson, G. L. *Phys. Rev. B* **1977**, *16*, 1889.
(37) Henling, L. M.; McPherson, G. L. *Phys. Rev. B* **1977**, *16*, 4756.
(38) Meyer, G. *Prog. Solid State Chem.* **1982**, *14*, 141.
(39) Barthem, R. B.; Buisson, R.; Cone, R. L. *J. Chem. Phys.* **1989**, *91*, 627.
(40) Seijo, L.; Barandiaran, Z. *J. Chem. Phys.* **2003**, *118*, 5335.
(41) Meyer, G. *Inorg. Synth.* **1989**, *25*, 146.
(42) Drożdżyński, J. *J. Less-Common Met.* **1988**, *138*, 271.
(43) Zych, E.; Drożdżyński, J. *Polyhedron* **1990**, *9*, 2175.
(44) Meyer, G.; Gaebell, H. C. *Z. Naturforsch. B* **1978**, *33*, 1476.
(45) Dereń, P. J.; Stręk, W.; Hanuza, J.; Zych, E.; Drożdżyński, J. *J. Alloys Compd.* **1995**, *225*, 114.
(46) Tanner, P. A.; Mak, C. S. K.; Faucher, M. D. *Chem. Phys. Lett.* **2001**, *343*, 309.
(47) Barandiaran, Z.; Seijo, L. *J. Chem. Phys.* **2003**, *118*, 7439.
(48) Faucher, M. D.; Moune, O. K.; Garcia, D.; Tanner, P. *Phys. Rev. B* **1996**, *53*, 9501.
(49) van Pieterson, L.; Reid, M. F.; Meijerink, A. *Phys. Rev. B* **2002**, *88*, 067405.
(50) Collombet, A.; Guyot, Y.; Mak, C. S. K.; Tanner, P. A.; Joubert, M.-F. *J. Lumin.* **2001**, *94−95*, 39.
(51) Karbowiak, M. Unpublished results.
(52) Schwartz, R. W.; Schatz, P. N. *Phys. Rev. B* **1973**, *8*, 3229.